Systems/Circuits

Mechanisms Underlying Population Response Dynamics in Inhibitory Interneurons of the *Drosophila* Antennal Lobe

Katherine I. Nagel and Rachel I. Wilson
Department of Neurobiology, Harvard Medical School, Boston, Massachusetts 02115

Local inhibitory neurons control the timing of neural activity in many circuits. To understand how inhibition controls timing, it is important to understand the dynamics of activity in populations of local inhibitory interneurons, as well as the mechanisms that underlie these dynamics. Here we describe the *in vivo* response dynamics of a large population of inhibitory local neurons (LNs) in the *Drosophila melanogaster* antennal lobe, the analog of the vertebrate olfactory bulb, and we dissect the network and intrinsic mechanisms that give rise to these dynamics. Some LNs respond to odor onsets ("ON" cells) and others to offsets ("OFF" cells), whereas still others respond at both times. Moreover, different LNs signal odor concentration fluctuations on different timescales. Some respond rapidly, and can track rapid concentration fluctuations. Others respond slowly, and are best at tracking slow fluctuations. We found a continuous spectrum of preferred stimulation timescales among LNs, as well as a continuum of ON–OFF behavior. Using *in vivo* whole-cell recordings, we show that the timing of an LN′s response (ON vs OFF) can be predicted from the interplay of excitatory and inhibitory synaptic currents that it receives. Meanwhile, the preferred timescale of an LN is related to its intrinsic properties. These results illustrate how a population of inhibitory interneurons can collectively encode bidirectional changes in stimulus intensity on multiple timescales, and how this can arise via an interaction between synaptic and intrinsic mechanisms.

Key words: *Drosophila* antennal lobe; inhibitory interneurons; intrinsic conductances; network dynamics; olfaction; synaptic dynamics

Significance Statement

Most neural circuits contain diverse populations of inhibitory interneurons. The way inhibition shapes network activity will depend on the spiking dynamics of the interneuron population. Here we describe the dynamics of activity in a large population of inhibitory interneurons in the first brain relay of the fruit fly olfactory system. Because odor plumes fluctuate on multiple timescales, the drive to this circuit can vary over a range of frequencies. We show how synaptic and cellular mechanisms interact to recruit different interneurons at different times, and in response to different temporal features of odor stimuli. As a result, inhibition is recruited over a range of conditions, and there is the potential to tune the timing of inhibition as the environment changes.

Introduction

One role of inhibitory interneurons is to control the timing of neural activity (Klausberger and Somogyi, 2008; Kerlin et al., 2010; Isaacson and Scanziani, 2011). Different interneurons in the same brain region can be recruited at different times during the same sensory or behavioral event (Lapray et al., 2012; Kvitsiani et al., 2013). Interneurons recruited at different times may have different effects on the network (Royer et al., 2012; Fukunaga et al., 2014). Inhibition is thus mediated by a constantly shifting ensemble of cells, and the timing of activity across the interneuron population is likely to be central to the function of these cells.

What mechanisms cause different interneurons to be recruited at different times? Interneurons in the same brain region can receive synaptic currents with different dynamics (Reyes et al., 1998; Glickfeld and Scanziani, 2006; Savanthrapadian et al., 2014). Even with a uniform pattern of current injection, interneurons can also exhibit diverse temporal patterns of spiking (Freund and Buzsáki, 1996; Markram et al., 2004; Tepper et al., 2010). Thus, both circuit and cellular mechanisms likely play a role. However, it has been challenging to link such mechanisms with *in vivo* activity.

Received Oct. 25, 2015; revised Jan. 9, 2016; accepted Feb. 2, 2016.

Author contributions: K.I.N. and R.I.W. designed research; K.I.N. performed research; K.I.N. analyzed data; K.I.N. and R.I.W. wrote the paper.

This work was supported by a research project grant from the US National Institutes of Health (R01 DC008174) and a Pathway to Independence Award from the US National Institutes of Health (K99 DC012065 to K.I.N.). R.I.W. is an Investigator of the Howard Hughes Medical Institute. We thank members of the Wilson laboratory for providing feedback on the paper.

The authors declare no competing financial interests.

Correspondence should be addressed to Dr. Rachel I. Wilson, Department of Neurobiology, Harvard Medical School, 220 Longwood Avenue, Boston, MA 02115. E-mail: rachel_wilson@hms.harvard.edu.

K. I. Nagel's present address: Neuroscience Institute, New York University School of Medicine, New York, NY 10016.

DOI:10.1523/JNEUROSCI.3887-15.2016

 0270-6474/16/364325-14$15.00/0

The *Drosophila* antennal lobe provides a simple model for investigating the dynamics and mechanisms of interneuron population activity. This circuit contains ~150 principal neurons and ~200 local neurons (LNs; Stocker et al., 1990; Chou et al., 2010). The antennal lobe is the first brain relay of the *Drosophila* olfactory system, and it shares the basic organization of the vertebrate olfactory bulb. Importantly, studies of interneurons and inhibition in the *Drosophila* antennal lobe have presaged subsequent findings in vertebrates (Hong and Wilson, 2013; Uchida et al., 2013; Zhu et al., 2013; Banerjee et al., 2015).

Most individual LNs in the *Drosophila* antennal lobe are broadly responsive to most odors, likely because they receive input from a broad group of excitatory neurons (Okada et al., 2009; Chou et al., 2010; Seki et al., 2010). Functional diversity in the LN population lies not primarily in their selectivity for odor identity, but in the dynamics of their odor responses. Different LNs respond to the same stimulus with different temporal patterns of spikes, and the response of a given LN tends to follow a similar time course, regardless of the chemical identity of the odor (Chou et al., 2010). The finding that LNs respond with different dynamics suggests that LNs might have different preferred stimulus timescales. The issue of stimulus timescales is particularly relevant in olfaction because odors tend to form filamentous plumes. From the perspective of an observer at one point in a plume, these filaments appear as temporal fluctuations at a wide variety of timescales (Murlis et al., 1992; Celani et al., 2014). However, LN responses to fluctuating stimuli have not been investigated systematically.

In this study, we investigate the timing of activity in the LN population, and the mechanisms that shape it. We show that LNs can encode either onsets or offsets in odor concentration (or both), and that LNs can be selective for different timescales of sensory input. LN population dynamics arise from an interaction between excitatory and inhibitory synaptic inputs and a variable intrinsic propensity to burst. Our findings provide a framework for thinking about the mechanisms and functions of ensemble dynamics among inhibitory interneurons.

Materials and Methods

Fly stocks. Flies were raised at 25°C on a cornmeal-agar-based medium under a 12 h light/dark cycle. All experiments were performed on adult female flies 1–3 d post-eclosion. Loose-patch recordings from GFP-positive LNs were made using the following genotypes:

GH298-Gal4,UAS-CD8:GFP
UAS-CD8:GFP;NP3056-Gal4
LCCH3-Gal4,UAS-CD8:GFP

We observed no statistically significant relationship between genotype and response properties, as measured by ON–OFF score or burst index, based on a one-way ANOVA. There was a small significant difference between the spontaneous firing rates of LNs expressing Gal4 under the control of the *LCCH3-Gal4* line versus the *NP3056-Gal4* line ($p = 0.02$, one-way ANOVA).

Whole-cell voltage-clamp recordings of odor-evoked currents (see Fig. 5) were performed mostly from LNs expressing GFP under the control of *GH298-Gal4*, with one recording using *NP3056-Gal4*. We chose to hold these cells at −40 mV and −60 mV in these experiments because more depolarized holding potentials tended to generate unclamped spikes, and more hyperpolarized holding potentials tended to degrade the recording quality over time. Recordings of EPSCs evoked by antennal nerve stimulation (see Fig. 6*A*,*B*) were made from GFP-positive LNs in the genotype [*Sco* or +]/[*SM6* or +];*NP3056-Gal4,UAS-CD8:GFP* or from GFP-positive PNs in the genotype *NP3481-Gal4,UAS-CD8:GFP*. Channelrhodopsin (ChR) experiments (see Fig. 6*C*–*F*) were performed in the genotype *UAS-H134R-ChR2/+;NP3056-Gal4,UAS-CD8:GFP*. "No ChR" controls were performed in flies that lacked the Gal4 transgene, namely the genotype *UAS-H134R-ChR2*. Both ChR-expressing flies and No-ChR control flies were reared in the dark in 6-oz culture bottles where the standard food was covered with a ⅛–¼ inch layer of rehydrated potato flakes mixed with a 35 mM stock solution of all-trans retinal (in ethanol, 50 μl). Current injection experiments in Figures 7 and 8 were performed in the genotype *GH298-Gal4,UAS-CD8:GFP*. All Gal4 lines and the LNs that they drive expression in were previously described (Stocker et al., 1997; Chou et al., 2010; Hong and Wilson, 2015; Nagel et al., 2015). The *UAS-H134R-ChR2* line was previously described by Pulver et al. (2009).

Photoionization detector recording. Photoionization detector recordings (Fig. 1*A*,*B*) were made using a miniPID (Aurora Systems). Values shown represent detector voltage. Because the photoionization detector (PID) generates small voltage responses for the odor stimulus we used in this study (2-heptanone at 1:100 dilution), we used a more concentrated stimulus for the PID recordings (2-heptanone at 1:10 dilution).

LN recording. LN recordings were made using standard techniques (Wilson and Laurent, 2005). Briefly, flies were anesthetized on ice and placed in a custom holder. For odor stimulation experiments, the antennae were positioned below the surface of the holder to keep them dry. The dorsal part of the head was bathed in external saline consisting of the following (in mM): 103 NaCl, 3 KCl, 5 TES, 8 trehalose, 10 glucose, 26 $NaHCO_3$, 1 NaH_2PO_4, 4 $MgCl_2$, and 1.5 $CaCl_2$. A window was cut in the cuticle over the dorsal part of the head to allow access to the brain, and the perineural sheath covering the antennal lobe was removed with fine forceps. The brain was visualized using an Olympus BX51 upright microscope with a 40× water-immersion objective and a fluorescence attachment containing a 100 W Hg arc lamp and a FITC/GFP LP filter cube (Chroma 41012). For whole-cell current-clamp recordings, patch pipettes (5–7 MΩ) were filled with a solution containing the following (in mM): 140 KOH, 140 aspartic acid, 10 HEPES, 1 EGTA, 1 KCl, 4 MgATP, 0.5 Na_3GTP, and 13 biocytin hydrazide. The pH of the internal solution was adjusted to 7.2 ± 0.1 and osmolarity to 265 ± 3 mOsm. For whole-cell voltage-clamp recordings, the internal solution contained 140 mM CsOH in place of KOH. For loose-patch recordings, standard patch pipettes were filled with either Cs-based internal or external saline diluted to the same osmolarity as our internal solution (265 ± 3 mOsm). To establish a loose-patch recording, positive pressure was released before encountering the cell to prevent formation of a tight seal, and weak negative pressure was used to gently draw the targeted cell toward the pipette. Loose-patch recordings were performed in voltage-clamp mode with the command voltage adjusted so that the holding current was essentially zero. Cells that showed evidence of membrane rupture (observed as a change in spike waveform and a relatively large holding potential) were discarded. All recordings were made using an Axopatch 200B amplifier (Molecular Devices). Recordings were low-pass filtered at 2 kHz before digitization at 10 kHz.

A caveat associated with our measurements of resting potential (see Fig. 8*D*,*E*) is the difficulty of accurately measuring resting potential in neurons with a high-input resistance, due to the substantial depolarizing effect of the seal current in small cells (Gouwens and Wilson, 2009). We controlled for this factor by applying a constant negative holding current to compensate for the seal current. We selected the holding current in each cell so that the whole-cell spontaneous firing rate was equivalent to the loose-patch spontaneous firing rate in that cell.

Some of the same LN recordings analyzed here were used in a set of published analyses focusing on activity summed across all LNs, rather than diversity across LNs (Nagel et al., 2015, their Fig. 5).

Odor stimulation. The fly was restrained in a horizontal platform that allowed the dorsal part of the head to be bathed in saline while the ventral part of the head (including the antennae and maxillary palps) and most of the body remained dry and exposed to odors. Odor stimulation was delivered through a rapidly switching three-way solenoid valve (LFAA1201610H, Lee Company) positioned close to the fly. A Teflon odor delivery tube (3 cm long, 1.5 mm inner diameter) was connected the outlet of the valve and the end of the tube was situated < 1 mm from the fly's head. Two miniature video cameras (Unibrain) were used to reliably

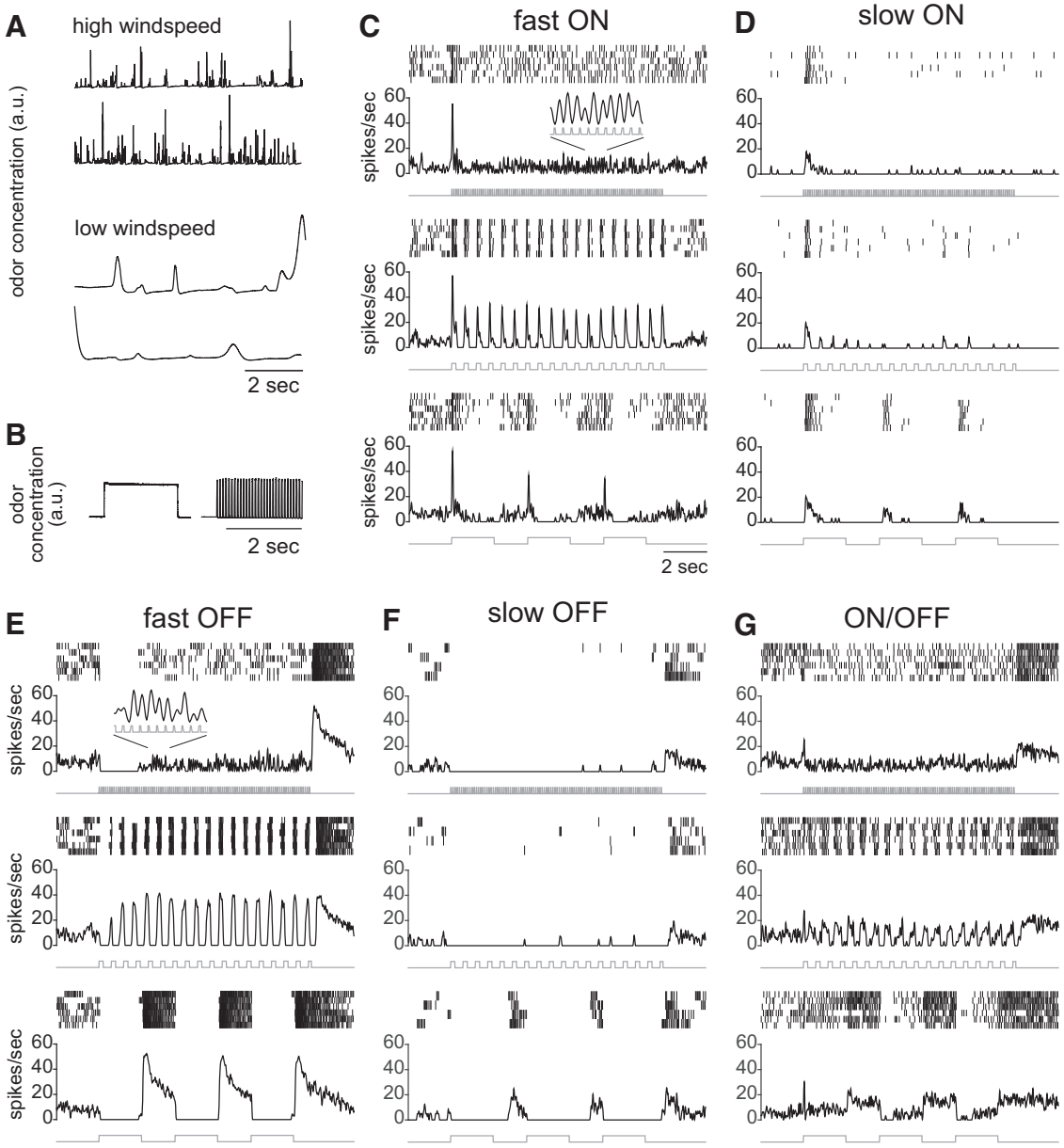

Figure 1. Odor fluctuations on many timescales and the diversity of LN responses in the time domain. ***A***, Odor concentration versus time in a turbulent plume, measured with a photoionization detector (arbitrary units but with consistent scaling in the top and bottom traces). From the perspective of a stationary odor sensor, lower wind speeds produce longer odor encounters, as well as longer intervals between encounters. ***B***, Odor concentration versus time, again measured with a photoionization detector (single trials) in response to a long (2 s) odor valve opening and also a 10 Hz train of brief odor valve openings (20 ms each). Note that the odor delivery system is able to deliver "artificial plumes" that are faithful to the pattern of odor valve opening. ***C***–***G***, Rasters and corresponding peristimulus time histograms show the spiking responses of five example LNs to three different stimuli. ***C***, A cell with a fast ON response that decreases over time. This cell responds quickly and can track rapid odor concentration fluctuations. Inset, Snippet of the response enlarged to show high-frequency tracking. ***D***, A cell with a slow ON response. This cell tracks slow but not fast odor concentration fluctuations. ***E***, A cell with a fast OFF response that facilitates over time. ***F***, A cell with a slow OFF response. This cell spikes in response to an odor concentration decrease, but only with a long delay; it is unable to track rapid fluctuations. ***G***, A cell that responds weakly at both onset and offset.

position the odor delivery tube for each experiment. On the day of the experiment, the odor 2-heptanone (Sigma-Aldrich) was freshly diluted 1:100 in 990 μl of paraffin oil and placed in a 1 ml screw-top vial. Air was charcoal-filtered and continually passed through the headspace of this vial at 0.7 L/min to generate a steady-state odor concentration $<$1:100. Normally, the valve diverted the odor stream into an open tube with a vacuum at one end (flow rate 0.6 L/min) to prevent contamination of room air. This apparatus was designed to produce rapid switching between odor and non-odor states with little distortion of the square pulse waveform. We verified that this device could perform as designed by measuring odor concentration using the PID with the inlet placed at the location of the fly (Fig. 1*B*).

Our odor stimulus set consisted of 18 binary waveforms having varied odor pulse durations and interpulse intervals. These stimuli used three odor pulse durations (20 ms, 200 ms, 2 s) and six interpulse intervals (80, 180, 380, 780, 1580, and 3180 ms) in all possible pairwise combinations, yielding a total of 18 stimulus waveforms. Three of these waveforms are featured in many figures.

Electrical stimulation of olfactory receptor neuron axons. The third segments of both antennae were removed with fine forceps just before opening the head capsule. The antennal nerve ipsilateral to the recorded projection neuron (PN) was drawn into a large-diameter saline-filled pipette and stimulated with 50 μs pulses using a stimulus isolator (AMPI, Iso-Flex) in constant current mode. The stimulus amplitude was adjusted for each experiment to

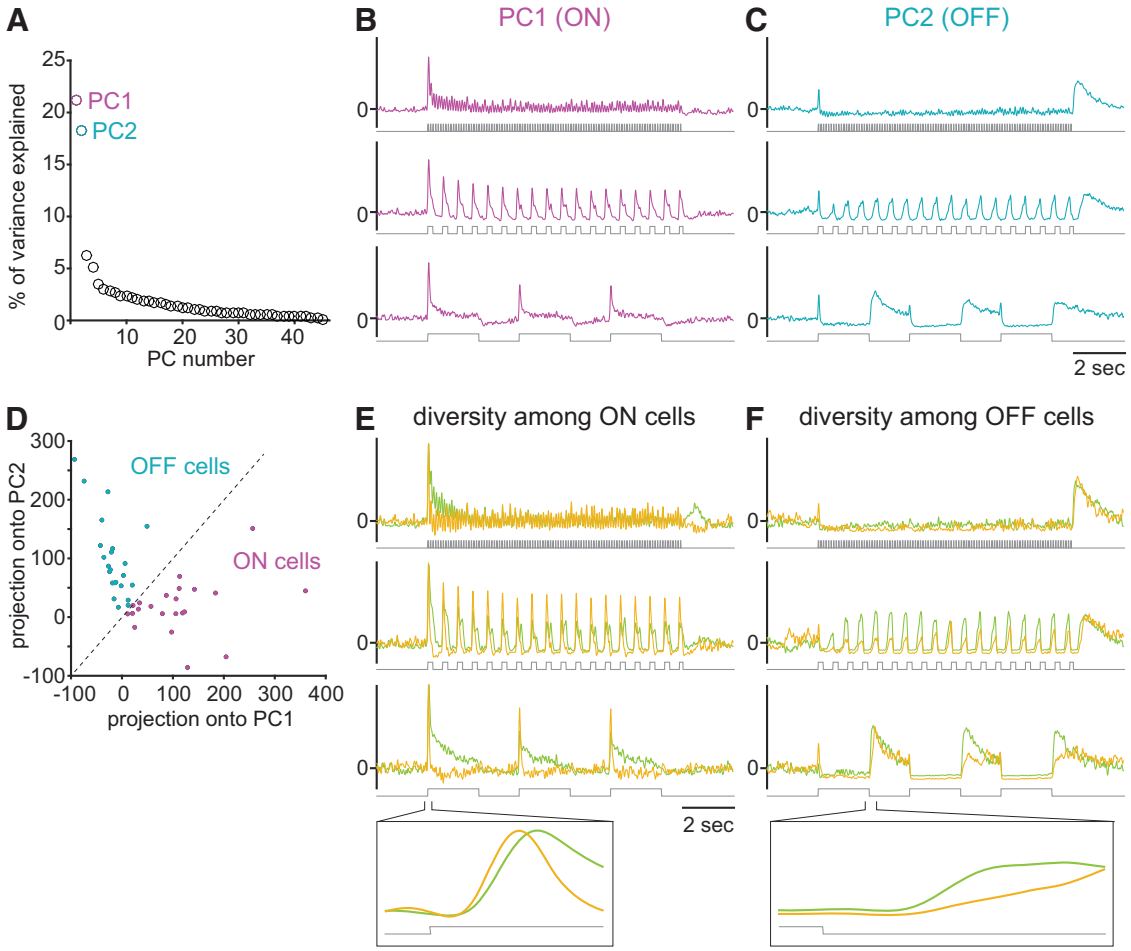

Figure 2. Describing the diversity of LN response dynamics with principal component analysis. ***A***, Scree plot showing variance accounted for by each PC. Two PCs accounted for a disproportionate fraction of the variance. PCA was performed on the set of 45 response vectors corresponding to 45 LNs. For each LN, firing rate responses to all 18 stimuli were concatenated to form a single vector. ***B***, The first PC resembles the response of a typical "ON" cell. Only the portion of the PC corresponding to the three stimuli shown in Figure 1 are shown (odor stimuli in gray). ***C***, The second PC resembles the response of a typical "OFF" cell. ***D***, Projections of all 45 LNs onto PC1 versus PC2. Cells were classified as ON (magenta) or OFF (blue) depending on whether they fell below or above the line of unity (dashed). Note that there is a continuum of response types, consistent with our observation that some cells show weak responses at both onset and offset. ***E***, Range of ON cell responses. Here we performed a second PCA on ON cells alone and plotted PC1 + PC2 (green) and PC1 − PC2 (gold) for the ON cell population, where each PC was normalized by the square root of the variance explained by that PC (see Materials and Methods). Both fast and slow ON responses appear in our data. Inset, A 200 ms snippet around odor pulse onset. ***F***, Range of OFF cell responses. Data analyzed and plotted as in ***E***, but for the OFF population. OFF cells also show a range of temporal profiles, but are somewhat less variable than ON responses. Inset, A 300 ms snippet around odor pulse offset. Note that PC1 + PC2 (green) happens to represent slow ON responses, but fast OFF responses.

produce a reliable EPSC waveform with minimal unclamped spiking (7.5–150 μA). Recordings with initial EPSCs larger than 80 pA tended to produce unclamped spikes, so we analyzed only recordings in which the initial EPSC amplitude was <80 pA.

Optogenetic stimulation of LNs. Channelrhodopsin-2 (H134R variant) was expressed under the control of *NP3056-Gal4*. This Gal4 line drives expression in a large and diverse population of GABAergic LNs (Chou et al., 2010). Within each antennal lobe, ~50 GABAergic LNs express Gal4, whereas the remaining ~50 GABAergic LNs do not (Chou et al., 2010). Light stimuli were provided by a 100 W Hg arc lamp, attenuated with a neutral density filter (30%), bandpass filtered at 460–500 nm, and delivered to the specimen focused through a 40× water-immersion objective. Light was gated by a shutter (Uniblitz) controlled by a TTL pulse.

Data analysis. All analyses were performed in MATLAB. Spikes were automatically detected as crossings of a threshold voltage, and were confirmed by visual inspection. After spikes were detected, voltage traces were filtered at 10 or 15 Hz to remove spikes and downsampled to 1 kHz before averaging and/or further analysis. For display purposes, traces were downsampled to 1 kHz without filtering. Peristimulus time histograms (PSTHs) were created by computing the average number of spikes per 1 ms bin over 1–6 trials of each stimulus, then smoothing with a 100 ms Hanning window centered at zero lag. In the insets below Figure 2*E–F*, we used the same filter but centered at a lag of 50 ms so that the filter was causal rather than acausal.

For principal component analysis (Fig. 2), we first computed PSTHs as described above, and then concatenated responses to all stimuli to form a single firing rate vector for each cell. The mean of each vector was set to zero (by subtraction) before analysis. Principal component analysis (PCA) was performed using the function PCA.m in MATLAB:

[pc c latent tsq scree] = pca(psth′,′centered′,0,′economy′,1);

where psth is a matrix in which each cell is a column and each time point is a row. PCA was performed without centering, meaning that the mean population response as a function of time was not subtracted from the data matrix before analysis. This ensured that the original responses could be reconstructed as linear combinations of the PCs. Projections onto each PC in Figure 2*D* were divided by the number of stimuli (18 stimuli in total) to facilitate comparison with later experiments where fewer stimuli were used to characterize each cell (Fig. 5D).

For the secondary PCA in Figure 2, *E* and *F*, we first classified cells as ON or OFF depending on whether they had a larger projection onto PC1 or onto PC2. We then performed PCA as above (without centering) on each category of LN responses. To illustrate the nature of the diversity

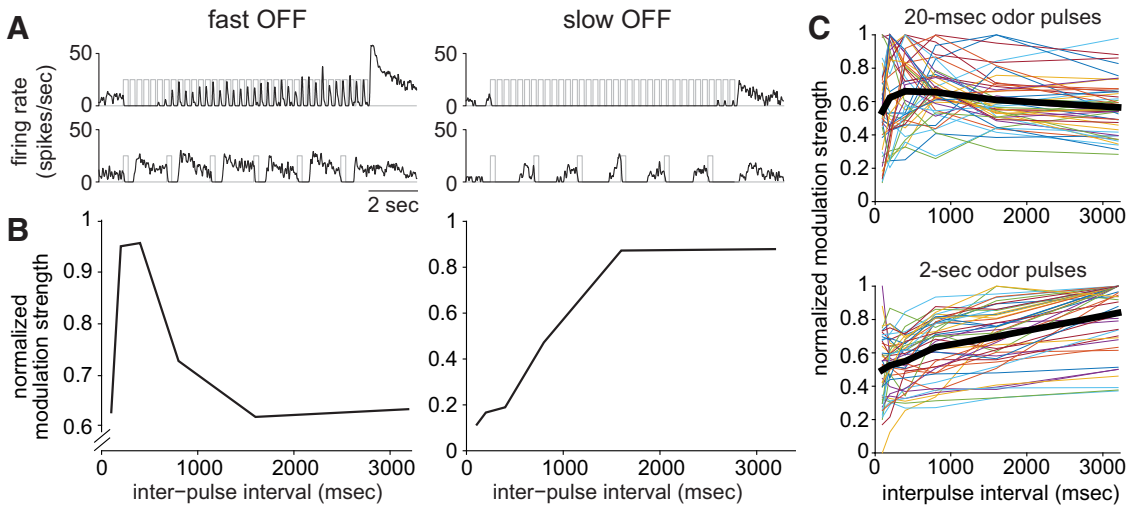

Figure 3. LN spikes lock more strongly to the stimulus when odor pulse duration scales with interpulse interval. ***A***, Two OFF cells responding to a stimulus with a short interpulse interval (top) and a long interpulse interval (bottom). One cell integrates on a short timescale (fast), the other on a longer timescale (slow). Odor pulses (gray) are 200 ms in duration. ***B***, For each stimulus, we computed the normalized modulation strength of the neural response. This metric quantifies how strongly the stimulus modulates a cell's firing rate (see Materials and Methods). A typical fast cell (left) shows the strongest modulation at short interpulse intervals, whereas a typical slow cell (right) shows strongest modulation at long interpulse intervals. Curves shown are for odor pulses 200 ms in duration. ***C***, Modulation strength for all cells, normalized to the maximum value for each cell. Data are shown for two pulse durations, 20 ms (top) and the 2 s. Cells are color-coded in the same way in the two plots. Thick black lines are averages across all cells. This analysis indicates that as a population, LNs show greater modulation in response to stimuli where the pulse duration and interpulse interval grow together. The preferred interpulse interval was significantly longer for 2 s pulses compared with 20 ms pulses ($p = 8.66 \times 10^{-4}$, *t* test).

within each category, we plotted the sum and the difference of the first two PCs, after first scaling each PC by the square root of the variance explained by that PC (ie, its SD). In other words, for both the ON and OFF categories, we plotted $(PC1 \cdot SD_{PC1}) \pm (PC2 \cdot SD_{PC2})$. This scaling procedure reverses the standardization imposed by the PCA calculation itself, so that the relative magnitude of the two PCs now corresponds to their weighting in the dataset. The resulting sum and difference illustrates the qualitative range of PSTHs within each category.

The ON–OFF index for each cell (see Fig. 5*D*) was calculated as its projection onto PC1, minus its projection onto PC2. The experiments in Figure 5 used only three of the stimuli from our full set of 18 stimuli (namely, 20 ms pulses with 80 ms intervals, 200 ms pulses with 380 ms intervals, and 2 s pulses with 1580 ms intervals). Therefore, to compute the projections onto PC1 and PC2, we used only the portions of PC1 and PC2 that corresponded to these three stimuli, and we divided the magnitude of the projections by the number of stimuli (three) to facilitate comparison with Figure 2*D*.

To compute modulation strength (Fig. 3), we first computed the average response over a single cycle of the stimulus (1 odor pulse plus 1 interpulse interval) and we subtracted the mean of this cycle average, yielding the average deviation over a cycle. We then computed the modulation strength as the norm of this vector (ie, the root of the sum of the squared deviations), divided by the stimulus period. Only full cycles were included in the analysis. The modulation strength was normalized to the maximum modulation strength for each cell, to permit the tuning of different cells to be compared more easily.

The "burst index" (Figs. 4, 8) was computed as the ratio of the mean interspike interval to the median. Total charge transfer (see Fig. 5*D*) was computed over the entire 10 s duration of three stimuli (20 ms pulses with 80 ms intervals, 200 ms pulses with 380 ms intervals, and 2 s pulses with 1580 ms intervals). In Figure 6*B*, average normalized EPSC amplitudes were fit to a simple depression model (Abbott et al., 1997; Tsodyks and Markram, 1997; Dayan and Abbott, 2001) where amplitude decreases by a factor f after each spike then recovers with time constant τ:

$$\text{if } s(t) = 1, A(t + \Delta t) = f * s(t) * A(t)$$

$$\text{if } s(t) = 0, A(t + \Delta t) = A(t) + (1 - A(t))\Delta t/\tau.$$

where $s(t)$ is a binary vector, sampled with a time step (Δt) of 1 ms that takes a value of 1 if a spike occurred in the presynaptic ORN and 0 otherwise. Rebound magnitude (see Fig. 7*B*) was computed by comparing the mean membrane potential or mean spike rate during the 2 s following stimulus offset to the membrane potential or spike rate during the 2 s before stimulus onset. The duration of the membrane potential response to a depolarizing current pulse (see Fig. 8) was computed by first filtering the membrane potential at 10 Hz to remove spikes, then computing the duration at half-maximum of the response following the current stimulus onset. Resting membrane potential (Fig. 8) was computed as the median membrane potential during epochs without a stimulus.

Results

Diverse response timing and selectivity for stimulation timescales in LNs

In nature, odors are often encountered in the form of turbulent plumes, where filaments of odor are interspersed with pockets of clean air (Murlis et al., 1992; Shraiman and Siggia, 2000; Celani et al., 2014). Turbulent plumes can contain odor concentration fluctuations on a wide range of timescales. The temporal scale of odor fluctuations depends on airspeed: high airspeeds produce brief, closely spaced odor encounters, whereas low airspeeds produce longer, more widely spaced odor encounters (Fig. 1*A*).

To ask how antennal lobe LNs respond to such stimuli, we measured the spiking responses of LNs using *in vivo* loose-patch recordings. Odors were presented to the fly using a rapidly switching valve that permitted fine temporal control of odor timing (Fig. 1*B*). We varied both the pulse duration and the interpulse interval to create a panel of 18 stimuli having a wide range of timescales (see Materials and Methods). We recorded from a total of 45 LNs in 38 flies using the same stimulus panel. In all these experiments, we used 2-heptanone as an odor stimulus, because it activates several types of olfactory receptor neurons and affects spiking in almost all antennal lobe LNs (de Bruyne et al., 2001; Chou et al., 2010). We made recordings from three different genotypes (see Materials and Methods) but observed no statistically significant difference in response properties between geno-

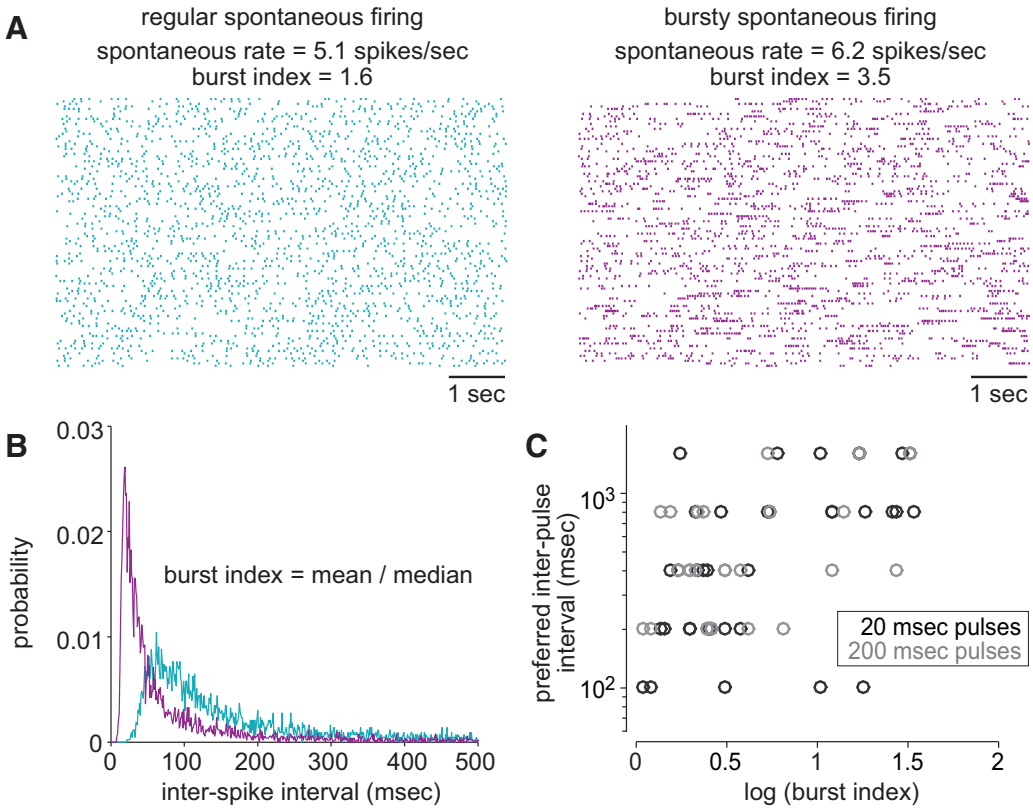

Figure 4. Spontaneous activity correlates with preferred odor pulse repetition rate. ***A***, Rasters showing spontaneous spiking activity in two example LNs, recorded in loose-patch mode. ***B***, The distribution of interspike intervals is different for these two cells. We defined the burst index as the mean interspike interval divided by the median interspike interval. A high burst index indicates a more bursty cell. ***C***, Over all the LNs in our sample, log(burst index) is positively correlated with preferred interpulse interval (the interval at which the cell's modulation strength peaks). This indicates that there is a relationship between a cell's preferred timescale of stimulation and its spontaneous activity. Data are shown for two different odor pulse durations (black: 20 ms, $r = 0.61$, $p < 0.0001$; gray: 200 ms, $r = 0.53$, $p < 0.0005$).

types. Therefore, we have pooled results from different genotypes in all analyses that follow.

When we presented a dense train of brief odor pulses, we found that most LNs were excited at either the onset or the offset of the train (Fig. 1*C–F*). We term these ON and OFF cells. When we presented a long odor pulse, ON cells responded most strongly to the onset of a long pulse (Fig. 1*C*,*D*), whereas OFF cells responded at pulse offset (Fig. 1*E*,*F*). ON responses typically decayed over the course of a pulse train or a long pulse. In contrast, OFF responses were more stable over time, or else they tended to grow. Many LNs fell along a continuum between ON and OFF. These intermediate cells responded to both stimulus onset and offset, and their peak responses were weaker than those of pure ON or OFF cells (Fig. 1*G*).

We also observed that different LNs were excited preferentially by stimulus fluctuations on different timescales. Some LNs responded with short latency and were able to track rapid pulse rates relatively accurately ("fast" cells). These cells also tended to have more transient responses to prolonged (2 s) pulses. Other LNs showed longer latencies to peak excitation and only responded repetitively when stimuli were longer and spaced further apart ("slow" cells). These cells tended to have more prolonged responses than did fast cells. We observed both fast and slow ON responses (Fig. 1*C*,*D*), and both fast and slow OFF responses (Fig. 1*E*,*F*).

A useful way to describe the difference between fast and slow LNs is to refer to the concept of "integration time." Fast LNs must have a short integration time to allow them to track rapid fluctuations. Slow LNs must have a long integration time to allow them to respond preferentially to slow fluctuations. We will explore the cellular correlates of integration time in more detail below.

It is notable that LN diversity is structured, not random: LNs do not represent all possible temporal features of an olfactory stimulus. For example, we never encountered ON cells whose firing rates grew over multiple odor pulses. We also never encountered OFF cells whose firing rates decayed over multiple odor pulses. In addition, we never observed stable and persistent responses to odor in any LNs. Rather, LNs are excited most strongly by changes in the olfactory environment, with different LNs signaling changes in different directions (increasing or decreasing odor concentration) and on different timescales (fast and slow).

Describing the space of LN diversity

To quantitatively describe the major types of variation in the LN population, we performed a principal component analysis (PCA). This analysis asks whether we can describe every LN response as a linear combination of a few component temporal patterns (PCs). The input to this analysis was a set of 45 vectors, corresponding to the responses of each of the 45 LNs from which we recorded. Spiking responses to all 18 stimuli were concatenated to form a single response vector for each LN.

This analysis revealed that the first two principal components (PC1 and PC2) accounted for a disproportionate amount of the variance in the data (Fig. 2*A*). These two PCs strongly resembled canonical ON and OFF responses (Fig. 2*B*,*C*). PC1 represents the

tendency for many cells to be excited at the onset of an odor concentration increase, whereas PC2 represents the tendency to be excited by an odor concentration decrease.

Notably, the ON PC (PC1) decayed over multiple odor pulses, whereas the OFF PC (PC2) was relatively steady over time, or even grew over multiple pulses (Fig. 2*C*, middle trace). In other words, PC1 and PC2 are not simply the inverse of each other (indeed, mathematically, they cannot be). Each has its own characteristic dynamics. PC1 captures the tendency for ON responses to decay over a prolonged stimulus or a long pulse train, whereas PC2 captures the tendency for OFF responses to grow over the course of a long pulse train.

To quantify how much each LN response resembled each of these PCs, we computed the projection of that LN′s firing rate vector onto PC1 and PC2 (Fig. 2*D*). Some LNs had large projections onto either PC1 or PC2, meaning they are ON or OFF cells, respectively. Other LNs had approximately equal but also small projections onto both PC1 and PC2, consistent with our finding that strong ON and strong OFF responses were mutually exclusive. LNs were continuously distributed in the space of these two PCs, representing a smooth continuum between ON and OFF behavior.

To describe the diversity within the ON and OFF categories, we assigned all cells to one of these categories depending on whether their projection onto PC1 or PC2 was greater. We then performed PCA separately on the ON and OFF categories of cells. This analysis showed that the major type of variation within each category was variation in integration time. ON responses ranged from fast and transient to slow and prolonged (Fig. 2*E*). Fast and transient responses were associated with strong phase locking to rapid stimulus modulations. OFF responses also showed a range of integration times, with faster rise times associated with better phase locking to rapid stimulus modulations (Fig. 2*F*).

This analysis supports the idea that there are two main types of variation in LN response dynamics. First, LNs vary in their selectivity for increases versus decreases in odor concentration. Second, LNs vary in the timescale over which they integrate changes in odor concentration. The distinction between ON and OFF cells corresponds to the first type of variation, and the distinction between fast and slow cells corresponds to the second.

Selectivity for natural stimulus configurations

As noted above, natural odor plumes occur on a wide range of timescales. In a turbulent plume, the interval between odor encounters tends to scale with odor encounter duration (Fig. 1*A*; Celani et al., 2014). In the laboratory, we can emulate "natural" stimuli where the pulse duration and the interpulse interval are approximately similar. We can also generate "unnatural" configurations in which long pulses are paired with much briefer interpulse intervals or vice versa. We wondered whether LNs exhibit stronger responses to more natural stimuli.

To quantify how strongly a given stimulus modulates a cell's firing rate, we used a metric we call the "modulation strength," defined as the root of the summed deviations from the cell's mean firing rate over a stimulus cycle period, divided by the period. Overall, we found that modulation strength was generally maximal at short interpulse intervals for fast LNs (Fig. 3*A*). Conversely, modulation strength was typically maximal at long-interpulse intervals for slow LNs (Fig. 3*B*).

We performed this analysis for two different odor pulse durations (20 ms and 2 s). We found that when pulse duration was short, the LN population as a whole tended to prefer short interpulse intervals. However, when the odor pulse duration was longer, the LN population shifted toward preferring longer interpulse intervals (Fig. 3*C*). We obtained qualitatively similar results when we used alternative metrics of phase-locking (eg, power at the stimulus frequency). This analysis argues that the LN population shows preferential tuning for natural odor concentration fluctuations, as compared with unnatural ones. Thus, although LNs are diverse, their diversity is structured to follow the statistical structure in odor concentration fluctuations.

Spontaneous bursting correlates with integration time

LNs spike spontaneously in the absence of odor stimuli (Chou et al., 2010; Nagel et al., 2015). In other circuits, spontaneous activity has provided clues to the mechanisms that shape stimulus-evoked activity (Kenet et al., 2003; Luczak et al., 2009). We therefore examined the dynamics of spontaneous activity in LNs.

Most LNs in our sample exhibited spontaneous spiking in loose-patch recordings (4.6 ± 2.8 spikes/s, mean ± SD). Some cells fired regularly, while others tended to show bursts of spikes (Fig. 4*A*). For each LN, we calculated a burst index, defined as the mean interspike interval divided by the median interspike interval. This index is high if the cell is bursty and low if the cell fires at regular intervals (Fig. 4*B*).

We found that spontaneous bursting was a good predictor of a cell's integration time in response to odor stimuli. Specifically, LNs that displayed regular spontaneous firing tended to phase-lock best to stimuli with shorter intervals between pulses. Conversely, LNs that displayed bursty spontaneous firing tended to prefer longer intervals between odor pulses. Overall, there was a significant correlation between a cell's preferred interpulse interval and the logarithm of its burst index (Fig. 4*C*).

Thus, spontaneous activity is predictive of odor stimulus integration time. Presumably, the same mechanisms that shape spontaneous dynamics are also priming the network to respond to stimuli with characteristic dynamics. We therefore investigated the mechanisms that distinguish the different functional types of LNs.

ON and OFF LNs receive different synaptic inputs

In principle, differences between LNs might arise from differences in synaptic input, or differences in intrinsic properties, or both. We began by recording both spikes and synaptic currents from many LNs, to test the hypothesis that ON and OFF cells receive different synaptic input.

In each experiment, we first recorded spiking responses to odors in loose-patch mode. We then established a whole-cell voltage-clamp recording, and once again presented the same stimuli to measure odor-evoked synaptic currents at a command potential of −60 mV. We used three stimulus waveforms in these experiments that sampled a range of stimulus configurations (the same as in Fig. 1).

These experiments revealed that ON and OFF LNs do indeed receive different synaptic input. In ON LNs, odor stimuli mainly elicited inward currents, indicating that excitatory synaptic input dominates these cells (Fig. 5*A*). Excitation was transient and was locked to stimulus onset.

In contrast, odor evoked mainly net outward (inhibitory) currents in OFF LNs, implying that synaptic inhibition dominates in these cells. In most OFF LNs, net current was actually inward (excitatory) for a brief period at stimulus onset, but then rapidly switched to outward for the duration of the stimulus (Fig. 5*B*). A similar switch was observed in cells with intermediate responses (weak ON and weak OFF), but these cells tended to have larger initial inward currents (Fig. 5*C*).

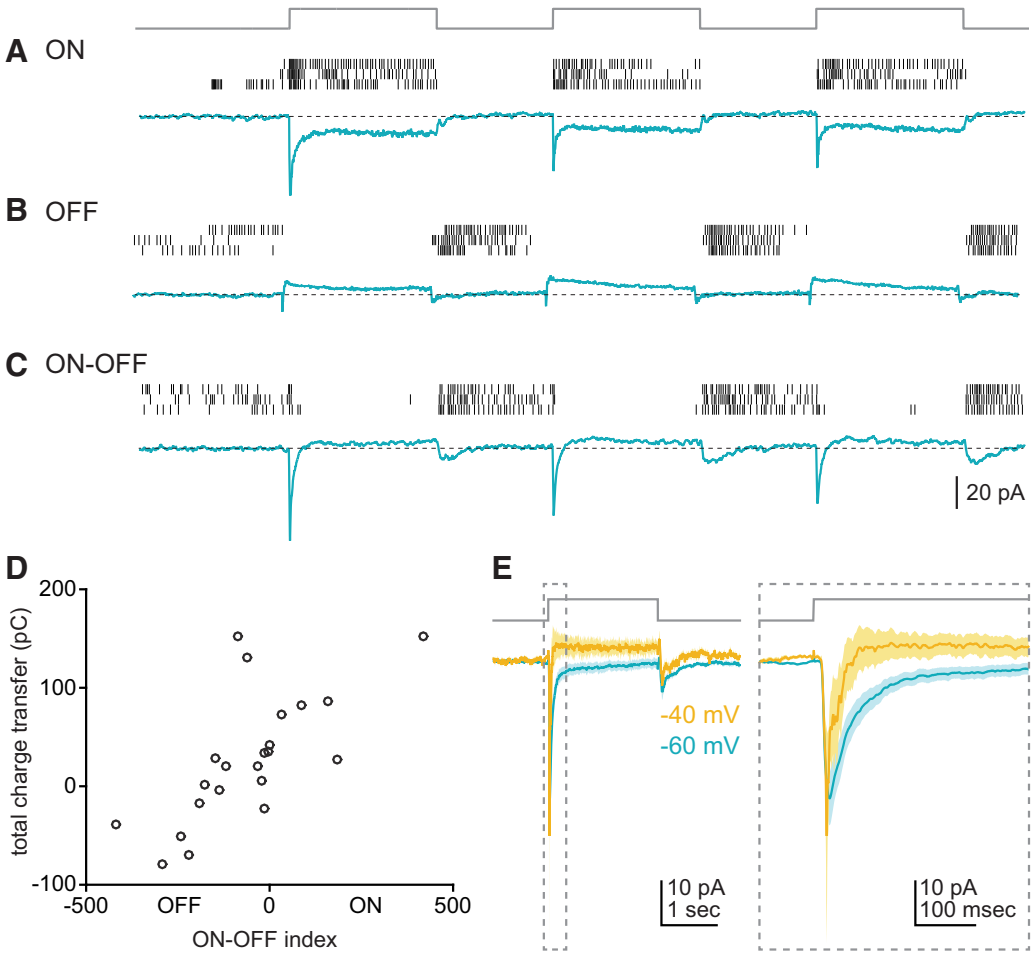

Figure 5. ON and OFF LNs receive different synaptic inputs. ***A***, An example ON cell recorded in both loose-patch and voltage-clamp modes. The stimulus was a series of 2 s odor pulses (top). Rasters (black) show spikes recorded in cell attached mode during three trials. Blue trace shows synaptic currents recorded while clamping the cell at −60 mV (averaged over 10 trials). Odor evokes a large net inward current that decays over time. ***B***, An example OFF cell recorded in the same manner. This cell shows a brief and small net inward current at the beginning of each odor stimulus that switches to net outward current for the duration of each odor pulse. ***C***, An intermediate cell. Here both odor onset and odor offset elicit a sizeable transient net inward current. ***D***, Total charge transfer versus ON–OFF index ($n = 22$). All cells were recorded sequentially in both loose-patch and whole-cell voltage-clamp modes. The ON–OFF index was calculated by projecting the spike rates recorded in loose-patch mode onto the first two principal components of the entire LN dataset (for the 3 stimuli used, shown in Fig. 1), and then subtracting the projection onto PC2 from the projection onto PC1. Total charge transfer was measured as the integral of the net change in holding current during all three stimuli (10 s of stimulus including odor pulses and intervals, holding potential = −60 mV). Total charge transfer is positively correlated with the ON–OFF index ($r = 0.69$, $p = 3.2 \times 10^{-4}$). ***E***, Odor-evoked currents measured at −60 and −40 mV, averaged across all cells recorded at both holding potentials ($n = 14$). Pastel bands are SEM. Right, Inset (enclosed in dashed lines) shows the response at odor onset on an expanded timescale.

To quantify the overall sign and magnitude of the synaptic currents in each cell, we measured the total charge transfer (ie, the integral of the whole-cell currents) over all three stimuli. For the same cells, we calculated an "ON–OFF index" by projecting the cell's spiking responses onto PC1 and PC2 (as in Fig. 2). We define the ON–OFF index as the size of the projection onto PC1, minus the size of the projection onto PC2. Thus, positive values of the ON-OFF index indicate ON behavior, and negative values indicate OFF behavior. Overall, we found a strong and significant correlation between total charge transfer and ON–OFF index (Fig. 5*D*). In cells where inward currents dominated, spiking occurred mainly at odor onset; in cells where outward currents dominated, spiking was suppressed by odor and increased at odor offset.

These results support the idea that ON and OFF cells receive, on average, different synaptic inputs. Both ON and OFF cells receive net inward current at stimulus onset, but OFF cells switch to net outward current by the end of the stimulus. What distinguishes ON from OFF cells is the relative magnitude and timing of inward and outward currents. We might therefore hypothesize that each cell receives both transient synaptic excitation and more slowly growing synaptic inhibition, but the balance of these two inputs varies between cells.

To test more directly the idea that excitation and inhibition have different dynamics, we recorded synaptic currents at two different holding potentials (−40 and −60 mV) in a subset of cells. At the more depolarized holding potential, outward currents became larger (Fig. 5*E*), indicating that these currents arise from synaptic inhibition, rather than the suppression of some tonic level of synaptic excitation. The time course of the net synaptic current also changed: the epoch of net excitation was more transient at the depolarized holding potential (Fig. 5*E*, inset). These results demonstrate that, on average, excitatory and inhibitory currents in LNs have different dynamics, and that during a prolonged odor stimulus, the balance progressively shifts toward inhibition.

Dynamics of excitatory and inhibitory synapses onto LNs

In most LNs, we observed a trend for synaptic excitation to shift to synaptic inhibition over the course of a long odor stimulus. In

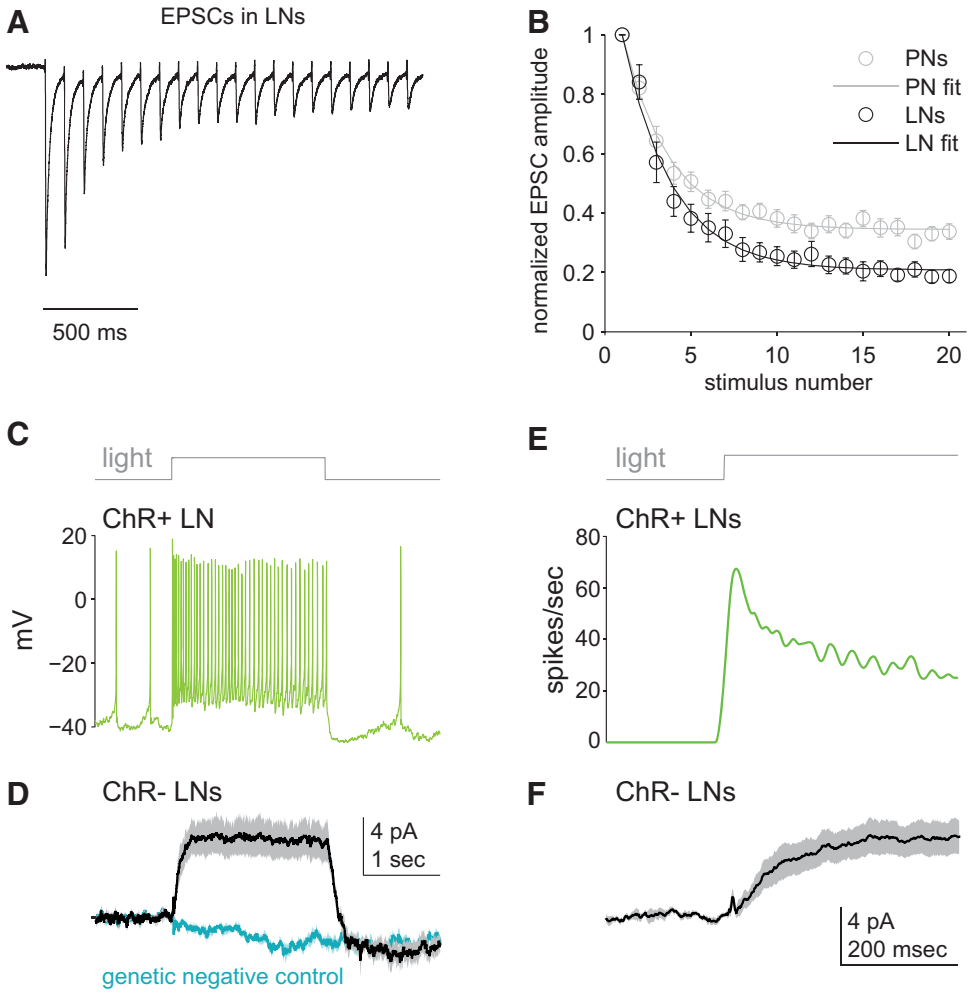

Figure 6. Dynamics of excitatory and inhibitory synapses onto LNs. ***A***, EPSCs recorded in LNs (mean of 9 cells) in response to electrical stimulation of ORN axons in the antennal nerve at 10 Hz. Note that EPSCs exhibit strong depression. ***B***, EPSC amplitude versus stimulus number for LNs and PNs (mean ± SEM, $n = 9$ for LNs and 19 for PNs). PN data are reproduced from Nagel et al. (2015). Lines are fits to a simple depression model where the amplitude of the unitary postsynaptic conductance decrements by a factor f after each spike and recovers with a time constant τ between spikes (see Materials and Methods). Values of f and τ are 0.75 and 1566 ms for LNs; 0.78 and 893 ms for PNs. ***C***, In a typical LN expressing channelrhodopsin-2 (ChR+), light evokes depolarization and spiking. Within each antennal lobe, ~50 GABAergic LNs expressed channelrhodopsin, whereas the remaining ~50 GABAergic LNs did not (see Materials and Methods). ***D***, Light-evoked spiking in ChR+ LNs elicits outward current in LNs that do not express channelrhodopsin (ChR−). In genetic controls where the Gal4 transgene was omitted (blue), there was essentially no effect of light. Traces are mean ± SEM across cells (black, with Gal4, $n = 9$; blue, no Gal4, $n = 6$). ***E***, Mean firing rate in ChR+ LNs (mean ± SEM across cells, $n = 5$). ***F***, Outward current in ChR− LNs, reproduced from ***D*** and shown on an expanded timescale. Note that outward currents in ChR− LNs grow slowly, even as firing rates are decaying in ChR+ LNs.

principle, this might reflect the time course of spiking in the excitatory and inhibitory neurons that provide input to LNs. LNs receive input from olfactory receptor neurons, antennal lobe projection neurons, and other LNs (Wilson et al., 2004; Huang et al., 2010; Yaksi and Wilson, 2010). All of these neurons have dynamical spike trains. However, we wondered whether part of the explanation might also lie in the dynamic properties of excitatory and inhibitory synapses themselves.

To explore this idea, we first investigated the dynamics of excitatory synapses onto LNs. To produce a controlled presynaptic spike train, we stimulated the severed axons of olfactory receptor neurons (ORNs) with electrical impulses at 10 Hz, evoking a train of EPSCs in voltage-clamped LNs. These EPSCs are likely dominated by direct excitation from ORNs, although there may also be a polysynaptic contribution from excitatory local circuits (Olsen et al., 2007; Huang et al., 2010; Yaksi and Wilson, 2010). We found that EPSCs exhibited strong short-term depression over the course of this train (Fig. 6*A*,*B*). Thus, the transience of excitatory currents in LNs may arise in part from the dynamics of excitatory synapses themselves. Notably, EPSCs measured in LNs showed more pronounced depression than those measured in PNs did. This difference may provide an explanation for why LN odor responses are more transient than are PN responses (Nagel et al., 2015).

Next, we investigated the dynamics of inhibitory synapses onto LNs. Odor-evoked inhibition in LNs presumably arises from other LNs. To produce a controlled pattern of activity in one group of LNs, while also recording synaptic inhibition from other LNs, we devised an optogenetic strategy. We expressed ChR in a large subset of LNs. Light-evoked spiking responses in ChR+ LNs had a rapid onset, and a prolonged light stimulus produced ongoing spiking with mild adaptation (Fig. 6*C*). When we recorded from LNs that did not express ChR, we observed light-evoked outward currents in these cells, indicating they received synaptic inhibition from the ChR+ LNs. Outward currents grew slowly over time, in contrast to the rapid onset of spiking in the ChR+ LNs (Fig. 6*D*–*F*). Note that

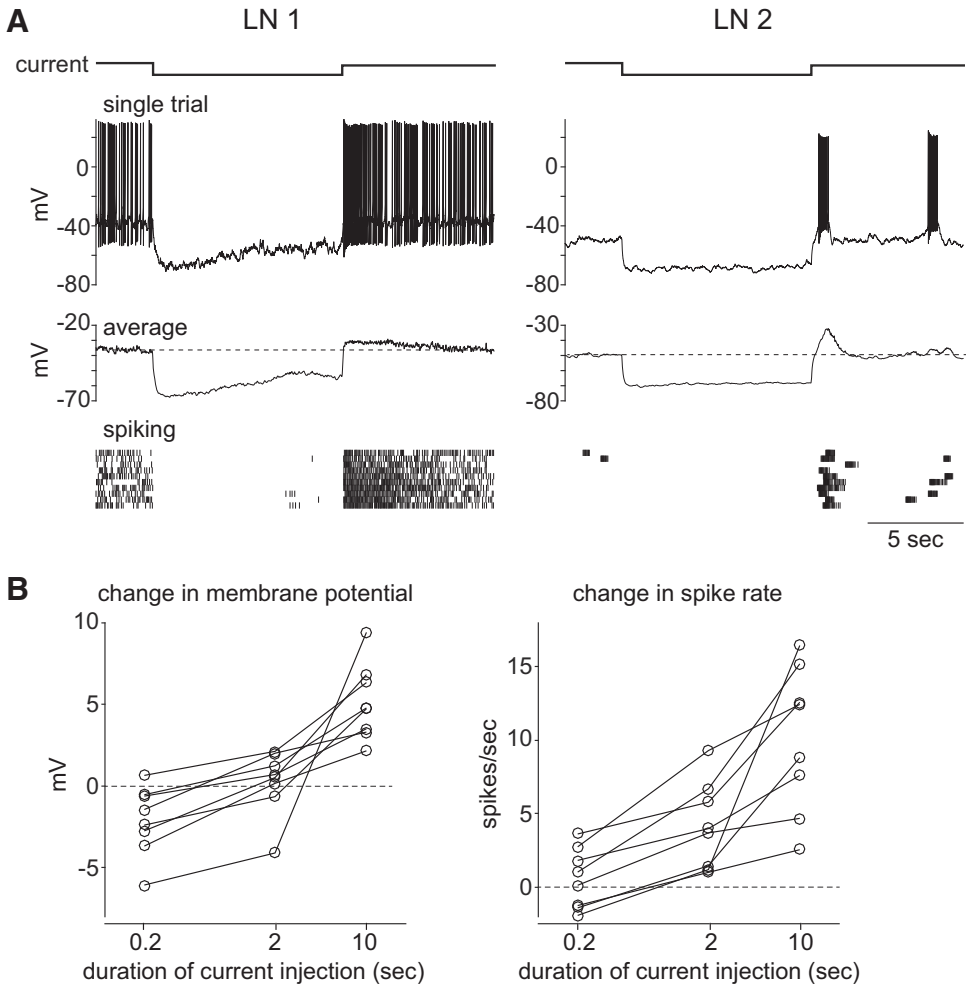

Figure 7. Intrinsic rebound amplifies OFF responses and facilitates over time. ***A***, Rebound firing in two example LNs in response to a 10 s injection of hyperpolarizing current (−20 pA). Top, single trials. Middle, membrane potential averaged across 10 trials (spike amplitudes are reduced by low-pass filtering before averaging). Bottom, Raster plot of spiking responses to current injection. Rebound depolarization and spiking was observed in eight of eight LNs. ***B***, Rebound grows with the duration of hyperpolarization. Membrane potential (left) and spiking responses (right) to hyperpolarizing currents of various durations (shown on a log scale). Each set of connected symbols represents a different cell. Responses were measured over 2 s following the end of the current pulse and are expressed relative to the 2 s before current injection.

although outward currents were growing, firing rates in the ChR+ LNs were in fact decaying slightly. This observation implies that there is some slowly growing process that intervenes between presynaptic spikes and postsynaptic inhibitory potentials. For example, neurotransmitter release from LNs might facilitate during a presynaptic train, or GABA might take some time to reach distant receptors.

In short, we find that excitatory synapses onto LNs are fast and depressing, whereas inhibitory synapses are slow and facilitating. These data are consistent with a model in which each LN receives a mixture of depressing excitation and facilitating inhibition, with the relative strength of excitation and inhibition varying across LNs.

Intrinsic rebound amplifies OFF responses

The synaptic inputs to LNs explain much of the distinction between ON and OFF cells, but not everything. In particular, OFF LNs fire at surprisingly high rates at stimulus offset, given that the net inward current in these cells is relatively small at odor offset (Fig. 5*B*). We therefore wondered whether the offset of odor-evoked hyperpolarization recruits an intrinsic rebound response that amplifies OFF responses.

To determine whether LNs show intrinsic rebound depolarization, we recorded from these cells in whole-cell current-clamp mode and injected prolonged hyperpolarizing currents via the patch pipette. At the offset of hyperpolarizing current, we observed rebound firing in all LNs tested (Fig. 7*A*). Rebound depolarization and rebound firing rates increased with the duration of hyperpolarizing current injection (Fig. 7*B*). The dependence of rebound firing on current duration was similar to the dependence of OFF LN firing on odor pulse duration (Fig. 1*E*,*F*). These data argue that OFF responses arise mainly from prolonged synaptic inhibition interacting with intrinsic voltage-dependent conductances.

Interestingly, rebound was not a property unique to OFF LNs. All the LNs we tested showed this property, and this sample included a mix of OFF cells, ON cells, and intermediate cells. There was a range of rebound amplitudes, but rebound occurred in all cells. Thus, all LNs are intrinsically competent to produce OFF responses, but rebound is stronger in some than in others, and only some of these LNs receive sufficient odor-evoked inhibition to generate a rebound burst. Because synaptic inhibition grows over time as LNs continue to spike (Fig. 6), and because intrinsic rebound also grows with more prolonged hyperpolarizations

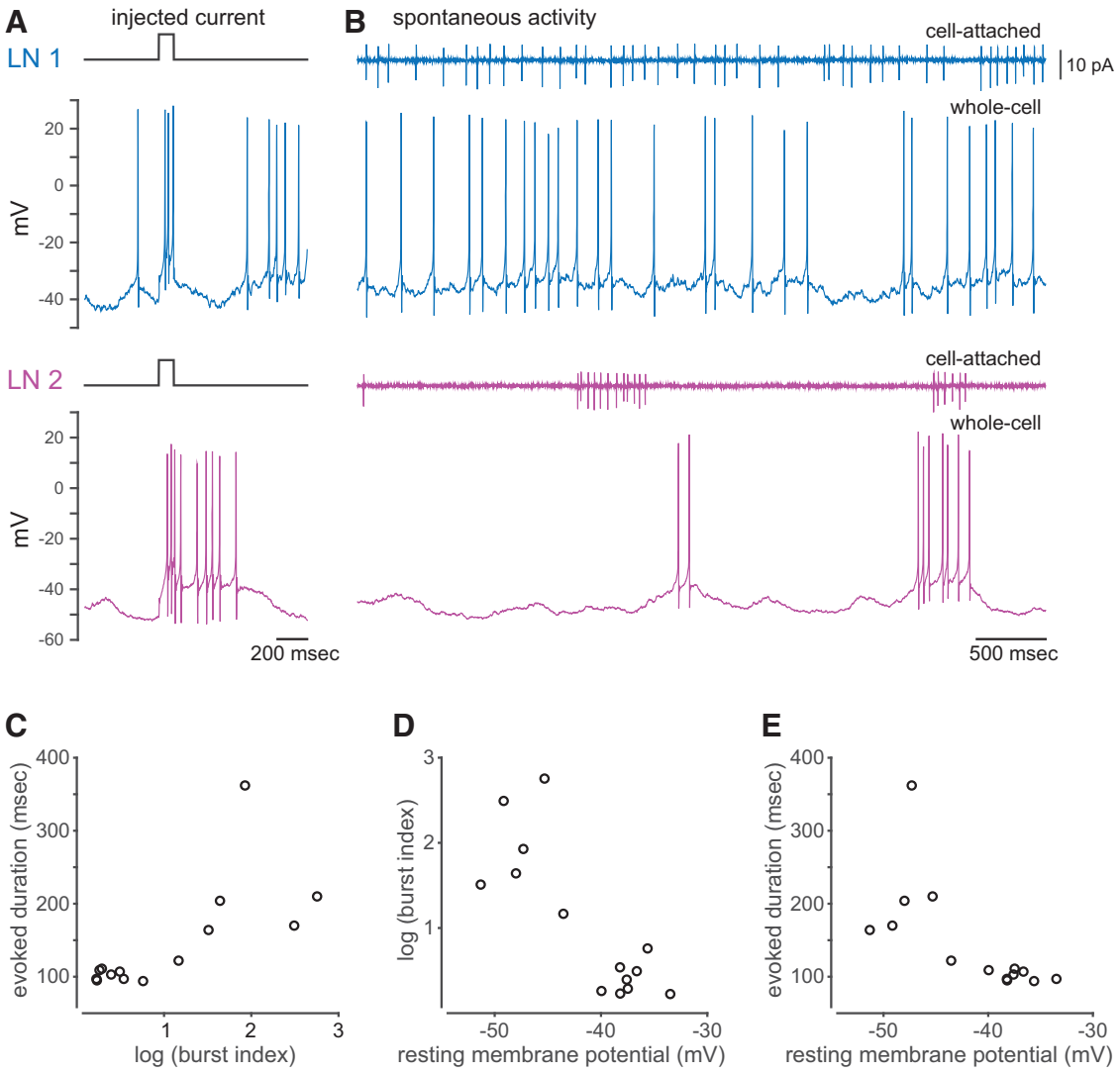

Figure 8. Intrinsic properties correlate with integration time. ***A***, Depolarization in two example LNs in response to 100 ms pulse of depolarizing current (20 pA). ***B***, Examples of spontaneous activity recorded in the same two LNs. For each cell, the top trace was recorded in loose-patch mode, the bottom trace in whole-cell mode. Burst indices were 1.6 and 4.5. ***C***, Duration of response to a 100 ms pulse of depolarizing current (20–30 pA) plotted versus log(burst index) ($n = 14, r = 0.71, p = 0.004$). Cells with regular spontaneous firing repolarize rapidly, whereas cells with bursty spontaneous firing repolarize slowly. ***D***, Log(burst index) versus resting membrane potential ($n = 14, r = -0.82, p = 3.4 \times 10^{-4}$). Overall, the resting potential of bursty cells is more hyperpolarized than that of regular-firing cells. ***E***, Duration of response to a 100 ms pulse of depolarizing current (20–30 pA) plotted versus resting membrane potential ($n = 14, r = -0.68, p = 0.0073$).

(Fig. 7), it is therefore logical that many OFF neurons exhibit spiking responses that become progressively larger during an ongoing odor pulse train, and that grow with increasing odor pulse duration (Figs. 1*E*, 3*A*).

Intrinsic properties correlate with integration time

We have found that there are two types of variation among LNs: ON versus OFF, and fast versus slow. Thus far, we have focused on the mechanisms that govern the distinction between ON and OFF cells. What creates the distinction between fast and slow cells?

Intrinsic conductances can shape both spontaneous activity and the dynamics of a neuron's response to synaptic input. We therefore wondered whether intrinsic mechanisms contribute to the difference between fast and slow LNs. To test this idea, we made whole-cell current-clamp recordings from a range of LNs with different response types, and examined responses to a brief depolarizing current injection (20–30 pA for 100 ms).

We observed that some LNs produced a brief depolarization after depolarizing current injection, whereas others produced a more prolonged depolarization (Fig. 8*A*). This result implies that intrinsic differences between LNs can contribute to variation in their integration time. Interestingly, LNs that depolarized briefly also generally fired regular spontaneous spikes. Conversely, LNs that depolarized for a prolonged period generally fired bursty spontaneous spikes. These features of spontaneous spiking behavior were observed in both loose-patch and whole-cell mode, meaning that they were not an artifact of the whole-cell recording configuration (Fig. 8*B*). Overall, there was a significant correlation between the logarithm of the burst index and the duration of the intrinsic response to depolarizing current injection (Fig. 8*C*). Thus, the distinction between regular-firing cells and bursty cells is due, at least in part, to differences in the intrinsic properties of these cells.

Interestingly, cells that were bursty and generated prolonged depolarizations also had more hyperpolarized resting

potentials. By contrast, cells that were regular-firing and fast to repolarize had depolarized resting potentials (Fig. 8*D*,*E*). This observation suggests that the distinction between fast and slow cells is due partly to the conductances that are open at rest in these cells. A hyperpolarized resting potential should deinactivate voltage-dependent sodium and calcium channels, which can lead to more bursting and a slower repolarization after the cell is stimulated.

Recall that spontaneous bursting is also correlated with a preference for longer odor stimulus intervals (Fig. 4*C*). This result implies that intrinsic mechanisms are at least partly responsible for creating the functional distinction between fast and slow LNs. Together, our results argue that intrinsic mechanisms play a role in generating tuning for long versus short interpulse intervals during a train of odor pulses, as well as in setting the integration time of the cell.

Discussion

Diverse temporal properties in inhibitory interneurons

In vivo, different inhibitory interneuron types are often activated at different times. This idea is supported by a growing number of recordings from the hippocampus, cortex, and olfactory bulb in awake animals (Lapray et al., 2012; Royer et al., 2012; Kvitsiani et al., 2013; Fukunaga et al., 2014). These studies show that different interneuron types can be recruited during different epochs of a sensory or behavioral event, or during different phases of rhythmic network activity.

Here we show that the same is true of the inhibitory interneurons of the *Drosophila* antennal lobe. Specifically, some interneurons responded selectively to odor concentration increases (ON cells), whereas others responded selectively to odor concentration decreases (OFF cells), or both (ON–OFF cells).

Moreover, some interneurons responded rapidly and transiently (fast cells). Others responded with longer delay, and their responses were also more prolonged (slow cells). Fast cells were preferentially recruited by high-frequency odor concentration fluctuations, whereas slow cells responded best to low frequencies.

In abstract terms, any time-varying signal can be described in terms of three parameters: frequency, phase, and amplitude, the latter here corresponding to odor concentration. The dynamics of odor concentration fluctuations are specified by their frequency and phase. Fast and slow neurons are preferentially recruited by different frequencies. Analogously, we can view ON and OFF neurons as being recruited at distinct phases. In this sense, the network of interneurons in this circuit can be seen as sampling the dynamical space of a time-varying odor stimulus. As a whole, the interneuron population responds to any deviation from the prevailing level of odor in the environment, with different neurons tracking deviations in different directions, and on different timescales.

Mechanistic basis of temporal diversity

We found that ON and OFF cells receive different synaptic inputs. In ON cells, the net odor-evoked synaptic current is inward, whereas in OFF cells it is outward. OFF behavior also depends on intrinsic voltage-gated conductances: prolonged hyperpolarization produces an intrinsic rebound, which leads to depolarization and spiking at odor offset. In other words, it is the interaction between synaptic and intrinsic conductances, which leads to spiking at odor offset in OFF cells. Notably, excitatory synapses onto LNs depress strongly. Conversely, inhibitory synapses onto LNs facilitate, as does intrinsic rebound. These mechanisms can account for why ON responses depress during a long train of odor pulses, whereas OFF responses tend to facilitate slightly.

In addition, we found that variation among cells in their frequency selectivity and integration time arises, at least in part, from differences in intrinsic conductances. Cells that prefer long intervals between odor pulses also tend to burst spontaneously. Spontaneously bursting cells rest at relatively hyperpolarized membrane potentials, and they display relatively prolonged depolarizations in response to current injection. Together, these results argue that the intrinsic properties of LNs are diverse, and this diversity helps create a wide range of integration times.

Previous studies have also found that there are multiple mechanisms underlying temporal diversity in interneurons. These studies have found that different interneuron types receive different synaptic inputs (Reyes et al., 1998; Glickfeld and Scanziani, 2006; Savanthrapadian et al., 2014) and display different intrinsic properties (Freund and Buzsáki, 1996; Markram et al., 2004; Tepper et al., 2010). Here we link these biophysical mechanisms with the diversity of LN responses to sensory stimuli *in vivo*. Moreover, we show how specific mechanisms are responsible for different axes of variation in the stimulus responses of LNs.

Implications of temporal diversity in interneurons

In considering the implications of temporal diversity in interneurons, it is useful to first review the proposed functions of the interneuron population in the *Drosophila* antennal lobe. One function is to control the gain of odor-evoked activity in antennal lobe PNs, in large part by regulating neurotransmitter release from presynaptic ORNs (Silbering and Galizia, 2007; Olsen and Wilson, 2008; Root et al., 2008; Asahina et al., 2009; Olsen et al., 2010). A second proposed function of inhibition is to shape the dynamics of odor-evoked activity in PNs so that it more faithfully reflects the dynamics of the stimulus itself (Nagel et al., 2015). A third proposed function is to precisely synchronize spike timing across PNs (Tanaka et al., 2009). All three functions require that inhibition be recruited at particular times, relative to activity in ORNs and PNs.

One possibility is that different local interneurons might perform essentially the same functions, but do so during different epochs of time. For example, fast LNs might be responsible for controlling PN gain when the stimulus is fluctuating rapidly. Conversely, slow LNs might be responsible for controlling gain when the stimulus is fluctuating slowly. Splitting this function among different neurons might provide a substrate for plasticity, as in the electrosensory lobe of the electric fish. In the electrosensory lobe, there is a large population of local interneurons (called unipolar brush cells) that each fire at characteristic times after a corollary discharge (Kennedy et al., 2014). These interneurons collectively create a temporal basis set which the network can use to learn the sensory consequences of a motor command. In this example, temporal diversity in an interneuron population allows that population to adapt its function as conditions change.

An alternative idea is that different interneurons might perform distinct functions. For example, ON LNs might contribute most to gain control. This would make sense, as they are the LNs that are most active when the excitatory drive to PNs is the strongest, ie, just after odor concentrations rise. Conversely, OFF LNs might have a different function, because their activity is actually suppressed when gain control is most needed.

Clues to the function of specific LN types might lie in their choice of postsynaptic targets. For example, a previous study had noted that some LNs are especially bursty (Seki et al., 2010). These bursty LNs innervate only the core region of each glomerulus, avoiding the rind where ORN axons terminate. It is therefore attractive to speculate that bursty LNs might avoid targeting ORNs, and might instead target other neurons.

To test these alternative hypotheses, it would be useful to have selective genetic access to functionally distinct LN types in the *Drosophila* antennal lobe. Previous studies have identified transgenic lines that drive expression groups of LNs that are moderately biased toward a particular LN type (Okada et al., 2009; Chou et al., 2010; Seki et al., 2010; Das et al., 2011). However, no studies have identified Gal4 lines that drive expression in a single LN type. Part of the problem is that we have lacked a clear framework for what might constitute a cell "type" within the LN population. In this study, we have developed a framework for classifying LNs. New technologies are likely to generate more selective genetic tools (Jenett et al., 2012). These tools, in parallel with the sorts of analyses we describe here, should allow us ultimately to understand the functions of population dynamics within inhibitory neuron networks.

References

Abbott LF, Varela JA, Sen K, Nelson SB (1997) Synaptic depression and cortical gain control. Science 275:220–224. Medline

Asahina K, Louis M, Piccinotti S, Vosshall LB (2009) A circuit supporting concentration-invariant odor perception in *Drosophila*. J Biol 8:9. CrossRef Medline

Banerjee A, Marbach F, Anselmi F, Koh MS, Davis MB, Garcia da Silva P, Delevich K, Oyibo HK, Gupta P, Li B, Albeanu DF (2015) An interglomerular circuit gates glomerular output and implements gain control in the mouse olfactory bulb. Neuron 87:193–207. CrossRef Medline

Celani A, Villermaux E, Vergassola M (2014) Odor landscapes in turbulent environments. Phys Rev X 4:041015. CrossRef

Chou YH, Spletter ML, Yaksi E, Leong JC, Wilson RI, Luo L (2010) Diversity and wiring variability of olfactory local interneurons in the *Drosophila* antennal lobe. Nat Neurosci 13:439–449. CrossRef Medline

Das A, Chiang A, Davla S, Priya R, Reichert H, Vijayraghavan K, Rodrigues V (2011) Identification and analysis of a glutamatergic local interneuron lineage in the adult *Drosophila* olfactory system. Neural Syst Circuits 1:4. CrossRef Medline

Dayan P, Abbott LF (2001) Theoretical neuroscience. Cambridge, MA: MIT.

de Bruyne M, Foster K, Carlson JR (2001) Odor coding in the *Drosophila* antenna. Neuron 30:537–552. CrossRef Medline

Freund TF, Buzsáki G (1996) Interneurons of the hippocampus. Hippocampus 6:347–470. Medline

Fukunaga I, Herb JT, Kollo M, Boyden ES, Schaefer AT (2014) Independent control of gamma and theta activity by distinct interneuron networks in the olfactory bulb. Nat Neurosci 17:1208–1216. CrossRef Medline

Glickfeld LL, Scanziani M (2006) Distinct timing in the activity of cannabinoid-sensitive and cannabinoid-insensitive basket cells. Nat Neurosci 9:807–815. CrossRef Medline

Gouwens NW, Wilson RI (2009) Signal propagation in *Drosophila* central neurons. J Neurosci 29:6239–6249. CrossRef Medline

Hong EJ, Wilson RI (2013) Olfactory neuroscience: normalization is the norm. Curr Biol 23:R1091–R1093. CrossRef Medline

Hong EJ, Wilson RI (2015) Simultaneous encoding of odors by channels with diverse sensitivity to inhibition. Neuron 85:573–589. CrossRef Medline

Huang J, Zhang W, Qiao W, Hu A, Wang Z (2010) Functional connectivity and selective odor responses of excitatory local interneurons in *Drosophila* antennal lobe. Neuron 67:1021–1033. CrossRef Medline

Isaacson JS, Scanziani M (2011) How inhibition shapes cortical activity. Neuron 72:231–243. CrossRef Medline

Jenett A, Rubin GM, Ngo TT, Shepherd D, Murphy C, Dionne H, Pfeiffer BD, Cavallaro A, Hall D, Jeter J, Iyer N, Fetter D, Hausenfluck JH, Peng H, Trautman ET, Svirskas RR, Myers EW, Iwinski ZR, Aso Y, DePasquale GM, et al. (2012) A GAL4-driver line resource for *Drosophila* neurobiology. Cell Rep 2:991–1001. CrossRef Medline

Kenet T, Bibitchkov D, Tsodyks M, Grinvald A, Arieli A (2003) Spontaneously emerging cortical representations of visual attributes. Nature 425:954–956. CrossRef Medline

Kennedy A, Wayne G, Kaifosh P, Alviña K, Abbott LF, Sawtell NB (2014) A temporal basis for predicting the sensory consequences of motor commands in an electric fish. Nat Neurosci 17:416–422. CrossRef Medline

Kerlin AM, Andermann ML, Berezovskii VK, Reid RC (2010) Broadly tuned response properties of diverse inhibitory neuron subtypes in mouse visual cortex. Neuron 67:858–871. CrossRef Medline

Klausberger T, Somogyi P (2008) Neuronal diversity and temporal dynamics: the unity of hippocampal circuit operations. Science 321:53–57. CrossRef Medline

Kvitsiani D, Ranade S, Hangya B, Taniguchi H, Huang JZ, Kepecs A (2013) Distinct behavioural and network correlates of two interneuron types in prefrontal cortex. Nature 498:363–366. CrossRef Medline

Lapray D, Lasztoczi B, Lagler M, Viney TJ, Katona L, Valenti O, Hartwich K, Borhegyi Z, Somogyi P, Klausberger T (2012) Behavior-dependent specialization of identified hippocampal interneurons. Nat Neurosci 15:1265–1271. CrossRef Medline

Luczak A, Barthó P, Harris KD (2009) Spontaneous events outline the realm of possible sensory responses in neocortical populations. Neuron 62:413–425. CrossRef Medline

Markram H, Toledo-Rodriguez M, Wang Y, Gupta A, Silberberg G, Wu C (2004) Interneurons of the neocortical inhibitory system. Nat Rev Neurosci 5:793–807. CrossRef Medline

Murlis J, Elkinton JS, Cardé RT (1992) Odor plumes and how insects use them. Annu Rev Entymol 37:505–532. CrossRef

Nagel KI, Hong EJ, Wilson RI (2015) Synaptic and circuit mechanisms promoting broadband transmission of olfactory stimulus dynamics. Nat Neurosci 18:56–65. CrossRef Medline

Okada R, Awasaki T, Ito K (2009) Gamma-aminobuyric acid (GABA)-mediated neural connections in the *Drosophila* antennal lobe. J Comp Neurol 514:74–91. CrossRef Medline

Olsen SR, Wilson RI (2008) Lateral presynaptic inhibition mediates gain control in an olfactory circuit. Nature 452:956–960. CrossRef Medline

Olsen SR, Bhandawat V, Wilson RI (2007) Excitatory interactions between olfactory processing channels in the *Drosophila* antennal lobe. Neuron 54:89–103. CrossRef Medline

Olsen SR, Bhandawat V, Wilson RI (2010) Divisive normalization in olfactory population codes. Neuron 66:287–299. CrossRef Medline

Pulver SR, Pashkovski SL, Hornstein NJ, Garrity PA, Griffith LC (2009) Temporal dynamics of neuronal activation by channelrhodopsin-2 and TRPA1 determine behavioral output in *Drosophila* larvae. J Neurophysiol 101:3075–3088. CrossRef Medline

Reyes A, Lujan R, Rozov A, Burnashev N, Somogyi P, Sakmann B (1998) Target-cell-specific facilitation and depression in neocortical circuits. Nat Neurosci 1:279–285. CrossRef Medline

Root CM, Masuyama K, Green DS, Enell LE, Nässel DR, Lee CH, Wang JW (2008) A presynaptic gain control mechanism fine-tunes olfactory behavior. Neuron 59:311–321. CrossRef Medline

Royer S, Zemelman BV, Losonczy A, Kim J, Chance F, Magee JC, Buzsáki G (2012) Control of timing, rate and bursts of hippocampal place cells by dendritic and somatic inhibition. Nat Neurosci 15:769–775. CrossRef Medline

Savanthrapadian S, Meyer T, Elgueta C, Booker SA, Vida I, Bartos M (2014) Synaptic properties of SOM- and CCK-expressing cells in dentate gyrus interneuron networks. J Neurosci 34:8197–8209. CrossRef Medline

Seki Y, Rybak J, Wicher D, Sachse S, Hansson BS (2010) Physiological and morphological characterization of local interneurons in the *Drosophila* antennal lobe. J Neurophysiol 104:1007–1019. CrossRef Medline

Shraiman BI, Siggia ED (2000) Scalar turbulence. Nature 405:639–646. CrossRef Medline

Silbering AF, Galizia CG (2007) Processing of odor mixtures in the *Drosophila* antennal lobe reveals both global inhibition and glomerulus-specific interactions. J Neurosci 27:11966–11977. CrossRef Medline

Stocker RF, Lienhard MC, Borst A, Fischbach KF (1990) Neuronal architecture of the antennal lobe in *Drosophila* melanogaster. Cell Tissue Res 262:9–34. CrossRef Medline

Stocker RF, Heimbeck G, Gendre N, de Belle JS (1997) Neuroblast ablation in *Drosophila* P[GAL4] lines reveals origins of olfactory interneurons. J Neurobiol 32:443–456. CrossRef Medline

Tanaka NK, Ito K, Stopfer M (2009) Odor-evoked neural oscillations in *Drosophila* are mediated by widely branching interneurons. J Neurosci 29:8595–8603. CrossRef Medline

Tepper JM, Tecuapetla F, Koós T, Ibáñez-Sandoval O (2010) Heterogeneity and diversity of striatal GABAergic interneurons. Frontiers in neuroanatomy 4:150. CrossRef Medline

Tsodyks MV, Markram H (1997) The neural code between neocortical pyramidal neurons depends on neurotransmitter release probability. Proc Natl Acad Sci U S A 94:719–723. CrossRef Medline

Uchida N, Eshel N, Watabe-Uchida M (2013) Division of labor for division: inhibitory interneurons with different spatial landscapes in the olfactory system. Neuron 80:1106–1109. CrossRef Medline

Wilson RI, Laurent G (2005) Role of GABAergic inhibition in shaping odor-evoked spatiotemporal patterns in the *Drosophila* antennal lobe. J Neurosci 25:9069–9079. CrossRef Medline

Wilson RI, Turner GC, Laurent G (2004) Transformation of olfactory representations in the *Drosophila* antennal lobe. Science 303:366–370. CrossRef Medline

Yaksi E, Wilson RI (2010) Electrical coupling between olfactory glomeruli. Neuron 67:1034–1047. CrossRef Medline

Zhu P, Frank T, Friedrich RW (2013) Equalization of odor representations by a network of electrically coupled inhibitory interneurons. Nat Neurosci 16:1678–1686. CrossRef Medline